

Giant flexoelectric effect in two-dimensional boron-nitride sheets

Ivan Naumov¹, Alexander M. Bratkovsky¹ and V. Ranjan²

¹*Hewlett-Packard Laboratories, Palo Alto, CA 94304, USA,*

²*North Carolina State University, Raleigh, NC 27606, USA*

(Dated: September 15, 2021)

We find, with the use of first-principles calculations, that a single-atom-thick boron-nitride (BN) sheet exhibits an unusual *nonlinear* electromechanical effect: it becomes macroscopically polarized when bent out-of-plane. The direction of the induced polarization is in the plane of the film and it depends non-analitically on the corrugation wave vector \mathbf{k} . The magnitude of the polarization can reach very high values in spite of being at least quadratic in atomic displacements due to BN sheets being able to tolerate large mechanical strains. The discovered effect can find many applications, in particular, in a new type of efficient and reliable nanogenerators.

PACS numbers: 61.46.Np, 77.55.+f, 77.80.-e, 77.84.-s

Three-dimensional (3D) bulk crystals can generate a voltage either in response to a mechanical strain $\partial_i u_l$ (piezoelectric effect [1, 2]) or to a strain gradient $\partial_i \partial_j u_l$ (flexoelectric effect [2, 3]), where $\mathbf{u}(\mathbf{r})$ is the displacement vector, with l its Cartesian index, ∂_i the gradient operator. The flexoelectric effect is usually small and evades experimental detection unless large strain gradients are externally imposed or artificially designed inhomogeneous metamaterials are used [3, 4]). It is commonly assumed that the effects *nonlinear* in $\partial_i u_l$ and $\partial_i \partial_j u_l$ on a polarization are negligible in bulk dielectrics.

Contrary to 3D systems, sp^2 -bonded 2D crystals, like graphene and boron nitride (BN) [5, 6], are able to sustain much larger structural distortions and, thus, exhibit new forms of electromechanical coupling. The BN sheet, for example, becomes pyroelectric when it is wrapped into a chiral or zigzag nanotube with the macroscopic polarization inversely proportional to the inverse square of the tube radius, $1/R^2$, and directed along the tube [7, 8, 9]. Formally, this effect can be considered as a *quadratic* flexoelectric effect since $1/R^2$ is only a particular form of $(\partial_i \partial_j u_k)^2$.

Here, we predict another unusual *nonlinear* electromechanical effect in 2D BN monolayer that has not been noticed so far: generation of a macroscopic *in-plane* polarization in response to out-of-plane atomic displacements like the corrugation $u_z(\mathbf{r}) = A \sin(\mathbf{k} \cdot \mathbf{r} + \varphi)$, where \mathbf{k} is the undulation wave vector, \mathbf{r} is the in-plane vector, z -axis is perpendicular to the plane, and φ is some phase. Although such displacements have *no* in-plane components and produce *zero* net curvature, they nevertheless induce an in-plane macroscopic polarization $\mathbf{P}(\mathbf{k})$, which is purely electronic in origin and related to the shifts of π and σ chemical bonds. It is remarkable that the induced polarization practically does not depend on the phase φ but strongly depends on wave vector \mathbf{k} , and there are some (“optimal”) directions along which the absolute value $|\mathbf{P}(\mathbf{k})|$ goes through a maximum. We show further that being at least quadratic in amplitude of atomic displacements A , the corrugation-induced polarization is decomposed basically into a sum of two contributions associated with the quadratic terms $(\partial_i u_k)^2$

and $(\partial_i \partial_j u_k)^2$, respectively. Whereas the first (“piezoelectric”) contribution can be understood starting from the piezoresponse of an isolated planar sheet, the second (“flexoelectric”) term has the same nature as the curvature-induced polarization in BN nanotubes, where $P \propto 1/R^2$.

It should be stressed that the discovered effect bears no relation to the formation of the *normal* polarization due to bending of 2D systems like graphene flat sheets where $P \propto 1/R$ [10, 11]. From a more general point of view, the effect can be considered as a mechanically-induced *improper* ferroelectric phase transition, with A playing a role of an order parameter. The externally imposed acoustic-phonon-like displacements $u_z(\mathbf{r})$ reduces the initially nonpolar symmetry group to some lower polar subgroup, so that $\mathbf{P}(\mathbf{k})$ is expanded in powers of A beginning with the term $\propto A^2$. Although $\mathbf{P}(\mathbf{k})$ is at least quadratic in A , the generated polarization can be very large provided that A is a fraction of the wavelength $2\pi/k$. The effect may find a variety of practical applications and, in particular, for conversion of the ambient wave-like micromovements into electricity: this tantalizing possibility is discussed below.

Among the truly 2D crystals that have been recently obtained using the so-called cleavage technique [12], boron-nitride monolayer is the only piezoelectric with wide band gap. Being partially ionic and partially covalent with sp^2 -bonding, a flat BN sheet has a remarkable mechanical flexibility associated with the ease of forming intermediate $sp^{2+\alpha}$ bonds. Due to its D_{3h} point symmetry group, it does not have a ground state polarization, although it exhibits piezoresponse with the piezoelectric tensor obeying the symmetry relations for the following non-vanishing components:

$$e_{x,xx} = -e_{x,yy} = -e_{y,xy} = -e_{y,yx}, \quad (1)$$

where x is directed along the symmetry axis of 2-th order [13].

To describe periodically and commensurately distorted hexagonal BN sheets, we introduce the corrugation wave vectors \mathbf{k} as $2\pi\mathbf{e}/\lambda$, where the unit vector \mathbf{e} and wavelength λ are expressed via the lattice vectors \mathbf{a}_1 and

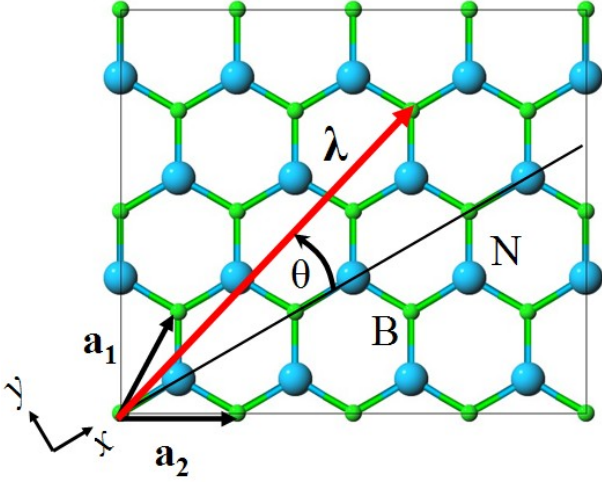


FIG. 1: Honeycomb BN lattice with basis vectors \mathbf{a}_1 and \mathbf{a}_2 . The x axis is chosen to be parallel to $(\mathbf{a}_1 + \mathbf{a}_2)$, whereas the y axis is perpendicular to it. The angle between the $(\mathbf{a}_1 + \mathbf{a}_2)$ and the chiral vector λ is the polar angle θ used in the paper to describe the corrugation wave vectors $\mathbf{k} = 2\pi/\lambda(n, m)$. The example corresponds to the case of $n = 3, m = 1$.

\mathbf{a}_2 of a 2D sheet in the following way: $\mathbf{e} = \lambda/\lambda$, with $\lambda(n, m) = n\mathbf{a}_1 + m\mathbf{a}_2$, $\lambda = a\sqrt{n^2 + nm + m^2}$, where n and m are integers, $a_1 = a_2 = a$ (Fig. 1). Note that the vector $\lambda(n, m)$ coincides with the chiral or circumferential vector defined in the theory of carbon nanotubes [5]. The corrugation with the wave-length $\lambda(n, m)$ leads to a rectangular supercell whose translational vectors are $\lambda(n, m)$ and some translation vector $\mathbf{T} = N\mathbf{a}_1 + M\mathbf{a}_2$, which is perpendicular to λ . The vector \mathbf{T} with length $T = a\sqrt{N^2 + NM + M^2}$ is completely defined by the vector λ [18]:

$$\mathbf{T} = \begin{cases} \sqrt{3}\lambda/p, & N - M \neq 3pq, \\ \sqrt{3}\lambda/(3p), & N - M = 3pq, \end{cases} \quad (2)$$

where p is the greatest common divisor of N and M , and q is an integer. It is also convenient to define the vectors \mathbf{k} in the polar coordinate system, (k, θ) , where θ is the angle between the \mathbf{k} and $(\mathbf{a}_1 + \mathbf{a}_2)$ [19]. We choose $(\mathbf{a}_1 + \mathbf{a}_2)$ in such a way that the shortest interatomic distance along this vector is passed from B to N atom (not from N to B, Fig. 1). Borrowing the terminology from the theory of nanotubes, we shall call the sine-wave distortions with $\theta = 0 \pm \pi l/3$ the “armchair”-like and with $\theta = \pi/6 \pm \pi l/3$ the “zigzag”-like, where l is an integer. All other distortions falling between the two will be called “chiral”.

To calculate the corrugation-induced polarization, we use the Berry-phase approach [14]. Namely, we treat the electronic polarization as a geometrical phase accumulated by the occupied electrons in the slow (adiabatic)

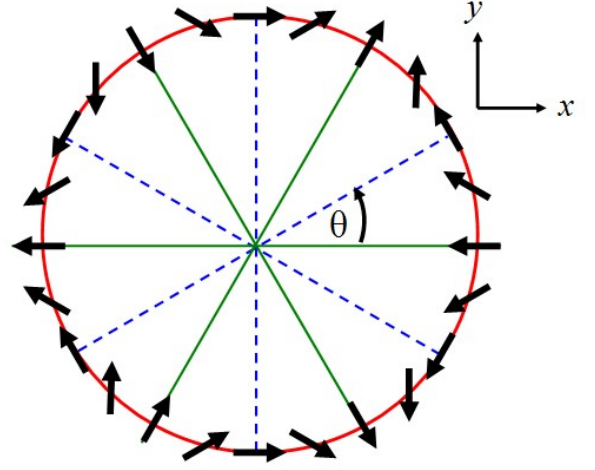


FIG. 2: A scheme showing the angular dependency of the polarization (depicted as arrows) induced by sinusoidal corrugations at a fixed “amplitude-to-wave-length” ratio Ak . While the \mathbf{k} -vector scans the angle θ from 0 to 2π , the Cartesian components of the polarization change approximately as $(-\cos 2\theta, \sin 2\theta)$, where θ is the angle defined in Fig. 1. Green solid and blue dashed lines indicate the armchair and zigzag directions along which the polarization is pure longitudinal and transverse, respectively.

process of corrugation: $\mathbf{P} = \mathbf{P}^{(u)} - \mathbf{P}^{(0)}$, with

$$\mathbf{P}^{(u)} = -\frac{2ie}{(2\pi)^2} \sum_{n=1}^M \int_{BZ} d^2\mathbf{k} \langle u_{n\mathbf{k}}^{(u)} | \nabla_{\mathbf{k}} u_{n\mathbf{k}}^{(u)} \rangle; \quad (3)$$

where $u_{n\mathbf{k}}^{(u)}$ is the periodic part of the Bloch functions and e is the electron charge. Note that the integral in this expression is taken over 2D Brillouin zone, so that the value of polarization has a dimension of a charge per unit length (electron charge per Bohr radius, e/a_B , if atomic units are used). Alternatively, in the simplest case of isolated bands, the formula (3) can be cast as

$$\mathbf{P}^{(u)} = -\frac{2e}{S^{(u)}} \sum_{n=1}^M \mathbf{r}_n^{(u)}, \quad (4)$$

where \mathbf{r}_n is the center of the Wannier function (WF) corresponding to the occupied band n and $S^{(u)} = \lambda T$ the surface area. Since the ionic contribution $(e/S^{(u)}) \sum_i Z_i \mathbf{R}_i^{(u)}$ to the total in-plane polarization does not change under the corrugations of interest, it can be completely neglected.

The integrals $\mathbf{P}^{(u)}$ (3) were computed using ABINIT code [15] with a $12 \times 4 \times 1$ Monkhorst-Pack \mathbf{k} -point grid, where the largest number 12 corresponds to the direction of undulations λ and 4 to the vector \mathbf{T} , perpendicular to λ . The flat and corrugated BN sheets were simulated by a slab-supercell approach with the interplanar distances of $20a_B$ and larger to ensure negligible

wave function overlap between the replica sheets. For the plane-wave expansion of the valence and conduction band wave-functions, a cutoff energy was used in the range of 80-100 Ry, depending on the corrugation wave length λ . The WFs and their geometrical centers $\mathbf{r}_n^{(u)}$ [see (4)] have been calculated with the PWSCF package [16] in three steps. First, we performed a self-consistent ground-state calculation and then a non-self-consistent calculation at fixed \mathbf{k} -points for all the occupied bands. And finally, the obtained Bloch functions were transformed into maximally localized WFs (MLWFs) as described in Ref. [17]. We used π and σ orbitals as initial guess projection functions allowing to obtain converged result for MLWFs. There are \mathcal{N} π -derived and $3\mathcal{N}$ σ -derived WFs, where \mathcal{N} is the number of B-N pairs per unit cell $\lambda \times T$.

Before describing the results of ab-initio modeling, we shall derive a phenomenological expression for $\mathbf{P}(\mathbf{k})$ considering the BN sheet as a continuous elastic membrane, which appears to be very accurate. Obviously, in the long-wave length limit ($\mathbf{k} \rightarrow 0$) the induced polarization can be expressed via 2D piezoelectric tensor components $e_{i,jk}$ and pure shear deformations, because isotropic distortions do not contribute to the polarization of a flat BN. Substituting the displacement field $u_z(\mathbf{r}) = A \sin(\mathbf{k} \cdot \mathbf{r} + \varphi)$ into the standard deformation tensor of a membrane [20]

$$\varepsilon_{ij} = \frac{1}{2} \left(\frac{\partial u_i}{\partial x_j} + \frac{\partial u_j}{\partial x_i} + \frac{\partial u_z}{\partial x_i} \frac{\partial u_z}{\partial x_j} \right), \quad (5)$$

where $x_i = (x, y)$, one can easily find the net shear components $\eta = (\varepsilon_{xx} - \varepsilon_{yy})/2$ and $\gamma = \varepsilon_{xy} = \varepsilon_{yx}$ as

$$\begin{pmatrix} \eta \\ \gamma \end{pmatrix} = \frac{\varepsilon_{\parallel}}{2} \begin{pmatrix} \cos 2\theta \\ \sin 2\theta \end{pmatrix}, \quad (6)$$

where $\varepsilon_{\parallel} = A^2 k^2 / 4$ is the net film stretch along the \mathbf{k} associated with the third term in Eq. (5) and θ is the angle related to \mathbf{k} the way shown in Fig. 1. The Cartesian components of polarization in the long wavelength approximation become $P_x = 2\alpha\eta$, $P_y = -2\alpha\gamma$, where α is the ‘clamped-ion’ piezoelectric constant $e_{x,xx}$ of a flat BN sheet. Using these components and relation (6), the vector of polarization can be presented as

$$\mathbf{P}(\mathbf{k}) = 2\varepsilon_{\parallel} (\mathbf{e}_{\parallel} \cos 3\theta - \mathbf{e}_{\perp} \sin 3\theta), \quad (7)$$

where \mathbf{e}_{\parallel} and \mathbf{e}_{\perp} are the unit vectors parallel and perpendicular to \mathbf{k} (\mathbf{e}_{\perp} are defined so that $\mathbf{z} \cdot [\mathbf{e}_{\perp} \times \mathbf{e}_{\parallel}] > 0$, $\mathbf{z} \parallel [\mathbf{x} \times \mathbf{y}]$). It is clear that the vector $\mathbf{P}(\mathbf{k})$ simply rotates with θ for the constant ε_{\parallel} .

Being accurate in the long-wave length limit ($\mathbf{k} \rightarrow 0$), the formula (7) must be corrected for shorter wavelengths by supplementing the terms $\propto k^4$. The first such term comes from the fact that the longitudinal component of polarization is tangent to the surface and tilted down and up relative to the initial (x, y) - plane. It, therefore, should be projected onto the plane, which has not been taken into account in Eq. (7). To obtain

this correction, one should average over λ the quantity $\frac{1}{2} \alpha A^2 k^2 \mathbf{e}_{\parallel} \cos 3\theta \cos^2(\mathbf{k} \cdot \mathbf{r} + \varphi) [\cos \vartheta(\mathbf{r}) - 1]$, where $\vartheta(\mathbf{r})$ is the tilting angle. Noticing that $\cos \vartheta(\mathbf{r}) - 1 \approx -\frac{1}{2} A^2 k^2 \cos^2(\mathbf{k} \cdot \mathbf{r} + \varphi)$ one can easily find the average as $-\frac{3}{32} \alpha A^4 k^4 \mathbf{e}_{\parallel} \cos 3\theta$.

The second correction accounts for the flexoelectric effect, i.e. the appearance of the macroscopic polarization due to finite curvature like in BN nanotubes. By symmetry, such a polarization is maximal in amplitude for the zigzag and minimal (zero) for the armchair directions; this angular dependence can be simply described by $\sin 3\theta$. Besides, the polarization should be parallel to \mathbf{e}_{\perp} , in close analogy with the tubes where the macroscopic polarization is always along the tube. And, finally, it should be proportional to the net inverse radius of curvature squared, $1/R^2$, instead of $1/R$ in the tubes. Defining the principal local curvature along the \mathbf{k} as $\nabla^2 u_z(\mathbf{r}) = A k^2 \sin(\mathbf{k} \cdot \mathbf{r} + \varphi) = 1/R(\mathbf{r})$, one can easily find that $1/R^2 \equiv \overline{R^{-2}} = A^2 k^4 / 2$. Thus, the curvature-induced correction can be represented as $\beta \overline{R^{-2}} \mathbf{e}_{\perp} \sin 3\theta$, where β is the flexoelectric constant.

By adding the above corrections to the expression (7), we come to the final result:

$$\mathbf{P}(\mathbf{k}) = \alpha \varepsilon_{\parallel} \left[\mathbf{e}_{\parallel} \left(1 - \frac{3}{2} \varepsilon_{\parallel} \right) \cos 3\theta - \mathbf{e}_{\perp} \sin 3\theta \right] + \beta \overline{R^{-2}} \mathbf{e}_{\perp} \sin 3\theta. \quad (8)$$

This formula is invariant with respect to rotation $\theta \rightarrow \theta + 2\pi/3$, as one would have expected from the D_{3h} symmetry. The first term comes from the increase in surface area that accompanies the sine-wave atomic displacements, it represents the piezoelectric effect. The second term, on the contrary, is non-zero only due to finite averaged curvature squared, obviously, it renders the flexoelectric effect. Since $\alpha < 0$ and $\beta > 0$, the extrema of the polarization are:

$$P_{\max} = |\alpha| \varepsilon_{\parallel} + \beta \overline{R^{-2}}, \quad \text{zigzag}, \quad (9)$$

$$P_{\min} = |\alpha| \varepsilon_{\parallel} \left(1 - \frac{3}{2} \varepsilon_{\parallel} \right), \quad \text{armchair}. \quad (10)$$

For all the other (chiral) directions, the amplitude falls within the above limits.

The calculations show that for relatively small $A/\lambda \lesssim 0.2$ the dependence $\mathbf{P}(\mathbf{k})$ does follow the continuous expression (8) very well. The mutual orientation of the \mathbf{P} and \mathbf{k} constantly evolves as the latter rotates through the angle θ (Fig. 2). \mathbf{P} becomes pure longitudinal along the armchair \mathbf{k} -directions and pure transversal along the zigzag directions. Along the chiral \mathbf{k} -directions, it has both components. Being practically independent of the initial phase φ , the magnitude of polarization P slightly depends on \mathbf{k} (within 30%) and reaches its minima along the armchair and maxima along the zigzag directions.

We have found α and β numerically to be $-0.118e/a_B$ and $0.044ea_B$, respectively. To check that the flexoelectric constant β is indeed related to the properties of BN

nanotubes, we considered a set of ‘ideal’ zigzag $(n, 0)$ nanotubes cut out of BN sheets in such a way that the B and N ions fall on the cylinder with radius R , $2\pi R$ coinciding with the ‘wave-length’ $\lambda(n, 0)$. These tubes are *longitudinally* polarized and their polarization is proportional to $1/R^2$ to a leading order in $1/R$. The coefficient of proportionality, as we found from additional calculations, is $0.042ea_B$, which is very close to the parameter β ($0.044ea_B$). This means that the curvature-induced polarizations in the corrugated BN sheets and in the BN nanotubes indeed have the same origin.

To analyze the relationship between electronic structure and $\mathbf{P}(\mathbf{k})$, we notice that the WF in a flat BN sheet have roughly the character of the σ - and π -bond orbitals (σ and π WFs). The π -like WFs are centered exactly on the N atoms, whereas their σ counterparts are somewhere in the middle of the B-N bonds closer to the N atoms (Fig. 3C). The contributions of the π and σ WFs to the ‘clamped-ion’ polarization induced by an in-plane uniaxial stretching have the *same* sign, with the π WFs dominating and amounting to as much as 85% of the total (see also Ref. [9]).

Although the corrugation of a flat BN sheet leads to the rehybridization effects like mixing of π and π^* electronic bands due to breaking the $z \rightarrow -z$ mirror symmetry [21], it is still possible to classify all the WFs into π and σ types, Figs. 3 and 4. It might naively appear that in the corrugated structures the main contribution to $\mathbf{P}(\mathbf{k})$ would also come from the π WFs. In fact, this is not the case. The contribution of σ WFs generally increases, becoming strongly dominant in some special cases in corrugated films.

Consider first the case of zigzag corrugation with $n = 4$, $m = -4$, $A/\lambda = 0.1$ and $\varphi = 0$, Fig. 3. Here, the shifts of π WFs are still dominant but not so apparently and $|P_\pi/P_\sigma|$ is only about 2.5. In contrast to the flat case, the π and σ WFs have the *opposite* sign contributions to $\mathbf{P}(\mathbf{k})$ exhibiting *inhomogeneous* shifts within the two-dimensional supercell $\lambda \times T$. Upon the corrugation, the π WF centers shift relative to the initial positions as shown in Fig. 3D. Although the sum of the shifts along the y axis cancels within the supercell, the similar sum along the x axis is nonzero, which means the appearance of a macroscopic transverse polarization, $\mathbf{P} \perp \mathbf{k}$. Interestingly, the magnitude of the shifts is larger in flatter and more stretched areas, and the shifts themselves (along y) are always directed towards more curved and less stretched areas. Because of the charge transfer from the flatter to curved regions, the conduction band maximum increases and the valence minimum increases in the curved areas, thus leading to a space modulation of the band gap with the wavelength λ .

Now, we turn our attention to another case, represented by the armchair undulation with $n = 4$, $m = 4$, $A/\lambda = 0.1$, and $\varphi = 0$, Fig. 4. Here again, the π and σ WFs give the *compensating* contributions to the polarization. But now, in contrast to the zigzag case, σ WFs dominate by a wide margin: $|P_\sigma/P_\pi| \sim 4.5$. All the WFs

shift strictly either along or opposite the \mathbf{k} -vector (Fig. 4C), so that the induced polarization is purely longitudinal. The dominant σ WFs move towards the N-atoms, thus further increasing the polarity of the σ B-N bonds. The magnitude of the shifts, as in the previous case, is larger in more flattened and stretched areas, but this works only in the second and fourth quarters of the λ . In the first and third quarters, the shifts of σ WFs are modest even in the well stretched areas. The charge transfer, therefore, increases the energy gap mainly in the second and fourth quarters at the expense of the first and third quarters of the wavelength.

Taking a reasonable amplitude-to-wavelength ratio of $A/\lambda \sim 0.2$, it is easy to estimate from Eq. (8) that the induced polarization can be on the order of $4 \times 10^{-2} e/a_B$. This quantity cannot be compared directly to that of 3D bulk materials because the latter has different dimension, e/a_B^2 . The comparison can be performed, nevertheless, if both 2D and 3D polarizations are expressed as the total dipole per stoichiometric unit [9]; then the polarization estimated above becomes $0.8ea_B$. It is tempting to compare this value with that in the standard perovskite $\text{PbZr}_x\text{Ti}_{1-x}\text{O}_3$ that has very high efficiency for converting electricity into mechanical strain and vice versa. Taking for the latter an experimental “bulk” piezoelectric constant e_{33} of 11.3 C/m^2 [23] and an achievable strain of 0.2% [24], we obtain only $0.2ea_B$, four times smaller than the one for BN (!). Hence, the generated polarization in a BN sheet can be comparable or even higher than that in best perovskite ferroelectrics. This situation pretty much resembles that in the field of electrostrictive materials. Usually, the electrostriction is a small effect, because the induced deformation is only *quadratic* in electric field or polarization. However, dielectrics with large polarization, such as the relaxor ferroelectric $\text{Pb}(\text{Mg}_{1/3}\text{Nb}_{2/3})\text{O}_3$ - PbTiO_3 , are capable of exhibiting the exceptionally large electrostrictive strains.

The important characteristic, the voltage drop U between opposite sides of the BN strip, can be estimated as $(P/\pi\epsilon\epsilon_0) \ln(L/b)$, where P is the usual 2D polarization (in units of C/m), L the separation between the charged strip edge states (strip width), and b the effective radius of those states, ϵ_0 the dielectric permittivity of vacuum. Taking b to be on the order of the lattice parameter a , for reasonable $L = (100 - 1000)a$, and $P = 10^{-2} e/a_B$, we formally obtain $U \lesssim 5 - 8 \text{ V}$ for BN strip suspended in vacuo and smaller values for the strip on dielectric substrate like SiO_2 ($\epsilon = 3.9$), or more than 20 times that of ZnO nanowires [29]. Interestingly, in case of suspended BN the band bending qU exceeds the value of the bandgap $E_g = 5.8 \text{ eV}$ [30], meaning that it will result in a charge transfer between the charged edges to make $qU \approx E_g$. This would mean that the achieved bias voltage would not depend on the strip width. For smaller bare values of the bias, it depends on L only logarithmically, i.e. very weakly. This insensitivity of the produced bias voltage is extremely attractive for applications. The ability of a BN sheet to effectively convert

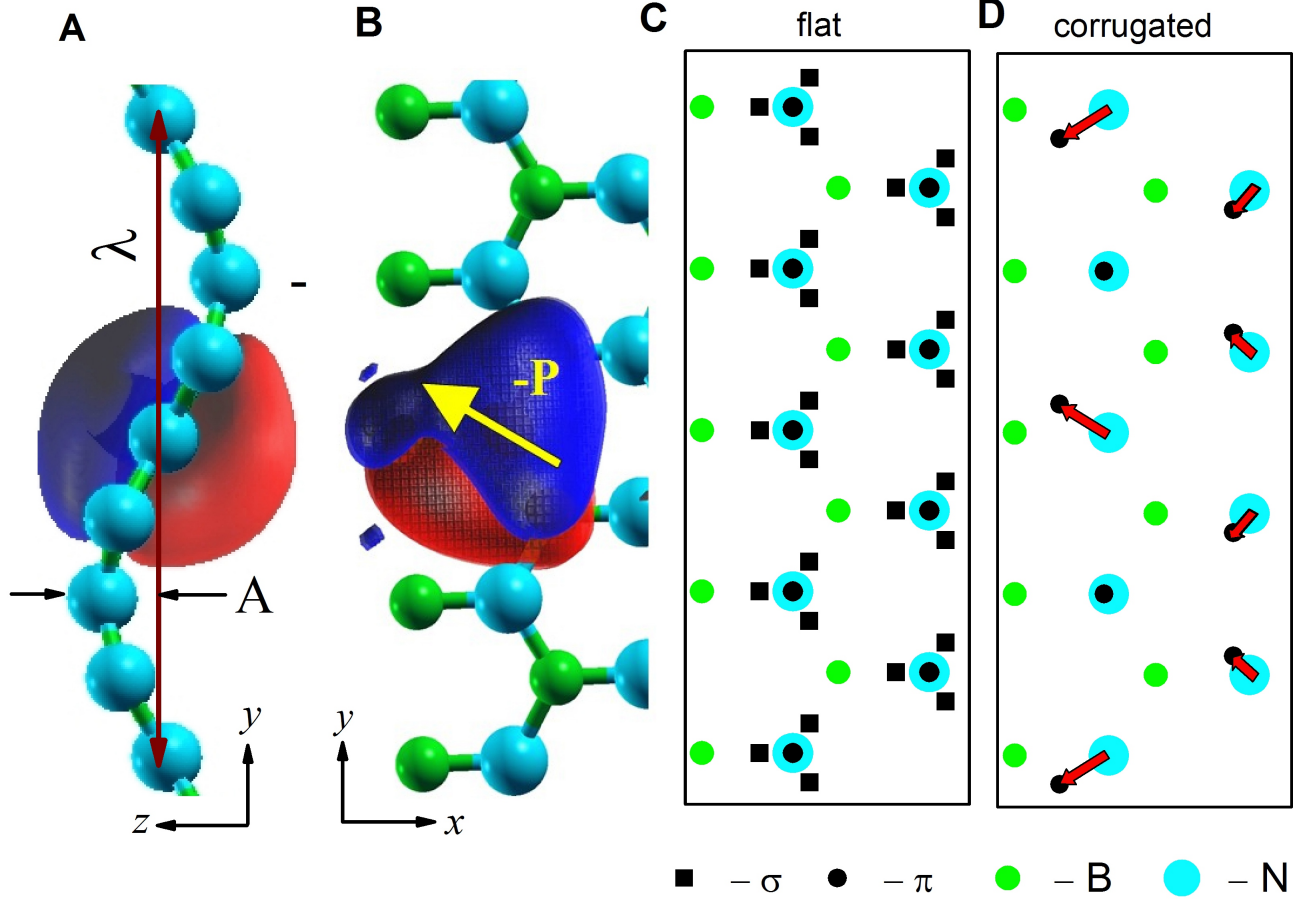


FIG. 3: Wannier functions and their shifts in a corrugated BN sheet corresponding to a zigzag period vector $\lambda(4, -4)$ ($\theta = 90^\circ$), $A/\lambda=0.1$, phase $\varphi=0$. (**A** and **B**) Side and top views of a π -like WF contributing most to the polarization (isosurface = ± 0.9). The yellow arrow indicate the shift of the WF in the (x, y) plane, which is antiparallel to the locally induced polarization \mathbf{P} . (**C** and **D**) The (x, y) - positions of the centers of the π and σ WFs in a flat and corrugated BN sheet, respectively. The positions of the centers of σ WFs are indicated by black squares, while those of π by black circles. In the initial flat state, the centers of π WFs coincide with those of N atoms. The red arrows show the most pronounced shifts in π WFs induced by the corrugation (the amplitudes of the shifts are tripled for clarity). Note that the yellow arrow points along one of the red ones.

wave-like deformations into electricity makes this material very promising for electromechanical applications at the nanoscale (Fig. 5). Below, we present a new concept of a nanogenerator powered by an ambient motion or agitation.

The direct and efficient conversion of mechanical energy into electricity is of great interest for practical applications. Recently, much attention has been attracted to the possibility of creating miniature nano-generators using semiconducting piezoelectric nanowires such as ZnO, GaN, and CdS [26, 27, 28]; during bending they generate the voltage bias between the opposite sidewalls. Unfortunately, such nanowires are not really suitable for this application. First, as has been pointed out in Ref. [29], they lose a significant fraction of their generated charges already in the process of bending due to large internal conductivity by virtue of being semiconducting. Second, since the nanowires are grown randomly, only a small

fraction of them (only about 1%) contributes to the generated electric current. And third, in order to generate a *dc* current, the nanowire should slide over a metallic electrodes until the nanowire/electrode interface becomes a forward-biased Schottky barrier; this is equivalent to a *ac-dc* converter.

The nanogenerator based on BN sheets does not suffer from all of the above shortcomings. First, the BN sheet is a dielectric nanostructure with a relatively wide energy gap (~ 5.8 eV). Second, all the atoms in the sheet are involved into producing electricity (it is the “bulk” effect). Third, the nanogenerator does not need any *ac-dc* converter, like a diode bridge rectifier, because the generated polarization has a *constant* direction provided that the direction of the wave vectors \mathbf{k} is fixed or, in other words, the ambient wave-like movements are oriented in the space. Fourth, the produced bias voltage is nearly independent from the BN strip width. Moreover, all these

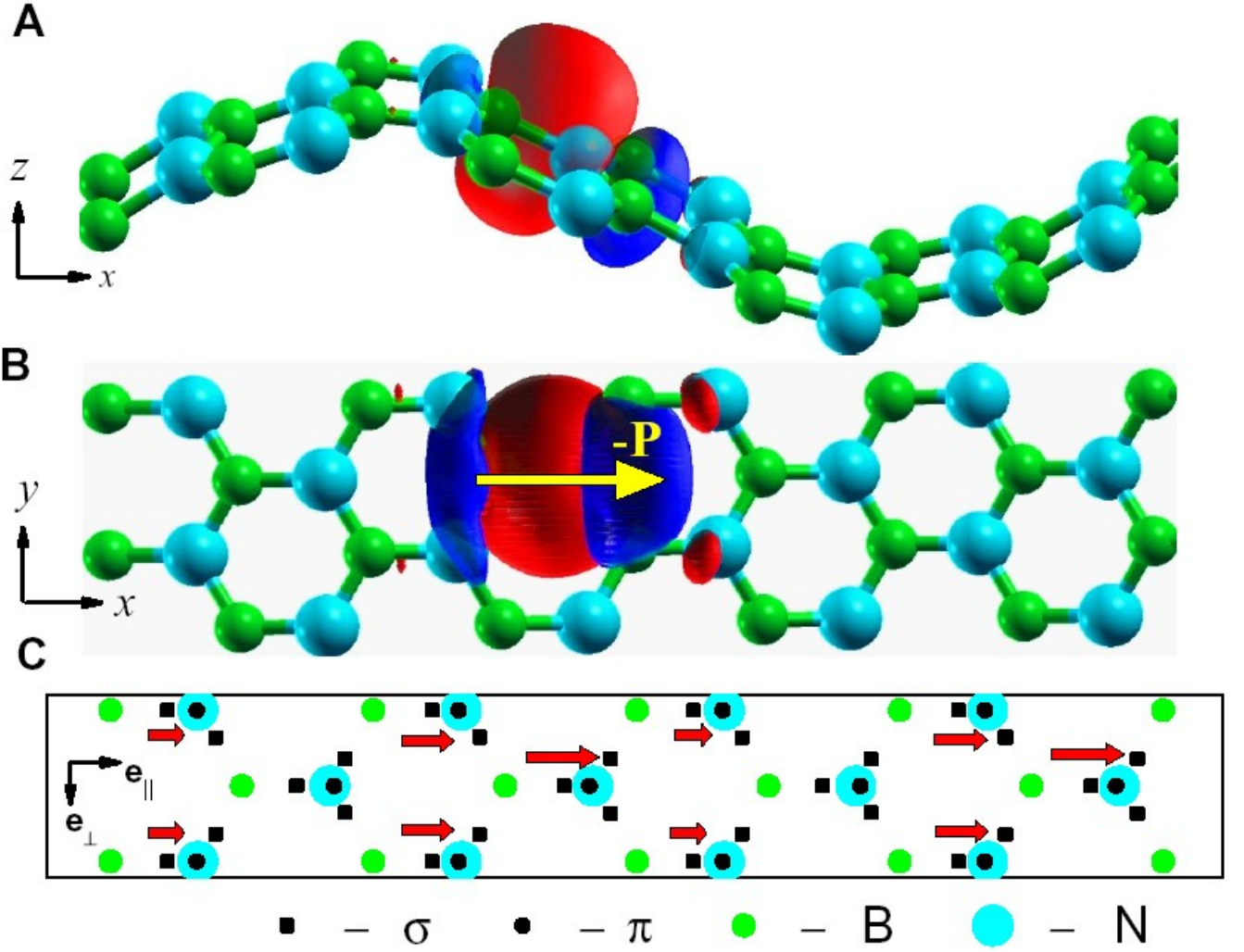


FIG. 4: Wannier functions and their shifts in a corrugated BN sheet corresponding to a armchair period vector $\lambda(4, 4)$ ($\theta = 0^\circ$), $A/\lambda=0.1$, $\varphi = 0$. (A and B) Side and top views of a σ -like WF contributing most to the polarization (isosurface = ± 0.9). The yellow arrow indicates the shift of the WF in the (x, y) plane, which is antiparallel to the locally induced polarization \mathbf{P} . The (x, y) - positions of the centers of the π and σ WFs in the corrugated BN sheet (C). The positions of the centers of σ WFs are indicated by black squares, while those of π by black circles. The red arrows show the most pronounced shifts in σ WFs induced by the corrugation (the amplitudes of the shifts are scaled up for clarity). Note that the yellow arrow corresponds to the red one.

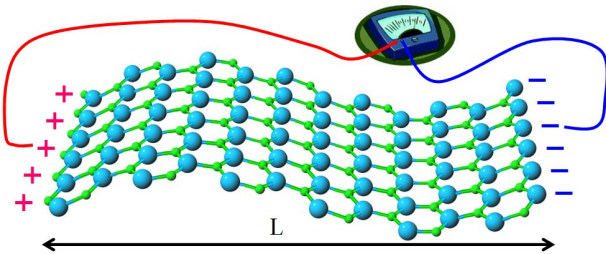


FIG. 5: Schematic showing generation of a bias voltage between the edges of a corrugated BN nanosheet (the geometry corresponds to Fig. 4). Note that the induced polarization is longitudinal, because the corrugation is of the armchair type (see text).

advantages couple with outstanding mechanical properties of a BN sheets, like their ability to be stretched or bent by several percent with no atomic defects involved [5].

It should be stressed that the corrugation-induced polarization can not be observed in a thin BN film cut out of the hexagonal bulk BN material. In such a film, the B and N arrangement is reversed in the neighboring hexagonal atomic layers, so that the polarization produced by each such pair of layers cancels out. However, the effect can be observed in an ultra-thin BN films with *odd* number of layers, 1, 3, 5, ... Here, of all the layers only one is going to produce the polarization, while the rest can be considered as a mechanically supporting substrate or scaffold.

It is worth mentioning that the BN monolayer is not the only 2D system capable of generating electricity under periodic bending. Its isoelectronic analog BC_2N exhibits similar effect in the ground state, like, for example, structure found with the LDA total energy calculations [31]. Due to absence of inversion symmetry, BC_2N in this structure is already polarized (electret) in the initial flat state with a polarization of $0.73 \times 10^{-2} e/a_B$ pointing along the armchair-type direction perpendicular to the pure C-C chains. Moreover, due to in-plane anisotropy under $2\pi/3$ rotations, the corrugation-induced polarization $\mathbf{P}(\mathbf{k})$ is no longer described by the formula (8) and its magnitude depends on θ much stronger than that in BN. Nevertheless, there are some \mathbf{k} -directions along which the generation of polarizations is practically as effective as in BN, such directions include the parallel and perpendicular ones to the above-mentioned C-C chains.

Here, we assumed that the edges of BN sheets are fixed and, therefore, the surface area of the membrane increases due to its deformation in the *third* dimension, and this increase is simply ε_{\parallel} . It is possible, however, to imagine the situation when the edges are not clamped and the layer bends in accordion-like fashion without any in-plane (average) stretching. In this case, the in-plane deformations $\partial_x u_y$ and $\partial_y u_x$ would cancel the nonlinear term $\partial_x u_z \partial_y u_z$ in Eq. (5), and the induced polarization would be defined *entirely* by the second, ‘flexoelectric’ term in (8). Such a polarization, however, is relatively modest because the elastic energy associated with the out-of-plane bending is noticeably smaller than the elastic stretching energy [22] (this, of course, is already evident from the comparison of the parameters α and β).

We have studied above the effectively infinite BN sheets satisfying the periodic boundary conditions, and the important question is whether the present results apply to the finite 2D BN systems. This question can be motivated by an example of a finite graphene sheet where the presence of zigzag edges induces the localized electronic states at each edge, thus modifying the properties of the initial infinite system [32]. Shall we expect the same effect in the case of BN? The answer is no, because, contrary to the carbon counterpart, the BN sheet does not have the conduction and valence bands that touch in a linear fashion at two inequivalent Dirac points, \mathbf{K} and \mathbf{K}' . This degeneracy is always lifted in a 2D BN due to a broken sublattice symmetry, so that the system remains insulating. In the present case the difference between \mathbf{P} in flat and electroded corrugated states in finite systems can be calculated by using periodic boundary conditions [33].

In summary, we have found that there is a strong polarization-corrugation coupling in a two-dimensional strip cut out of BN sheet, which can be decomposed into the nonlinear ‘piezoelectric’ and the flexoelectric effects. The direction of the induced polarization strongly depends on the corrugation wave vector \mathbf{k} and changes approximately as $(-\cos 2\theta, \sin 2\theta)$, where θ is the angle between the zigzag axes and \mathbf{k} . The magnitude of the polarization as a total dipole moment per chemical formula can reach very large values comparable to those in the best known perovskite piezoelectrics. The present effect may be used in nanoscale generators activated by ambient vibrations that can power small electronic devices and circuits.

-
- [1] R. Martin, Phys. Rev. B **5**, 1607 (1972).
 - [2] A. K Tagantsev, Phys. Rev. B **34**, 5883 (1986).
 - [3] L. E. Cross, J. Mater. Sci. **41**, 53 (2006).
 - [4] N. D. Sharma, R. Maranganti, P. Sharma, J. Mech. Phys. Solids **55**, 2328 (2007).
 - [5] R. Saito, G. Dresselhaus, M.S. Dresselhaus, *Physical Properties of Carbon Nanotubes* (Imperial College, London, 1998).
 - [6] J. C. Meyer *et al.*, Nature **446**, 60 (2007).
 - [7] E.J. Mele, P. Král, Phys. Rev. Lett. **88**, 056803 (2002).
 - [8] S. M. Nakhmanson, A. Calzolari, V. Meunier, J. Bernholc, M. B. Nardelli, Phys. Rev. B **67**, 235406 (2003).
 - [9] N. Sai, E. J. Mele, Phys. Rev. B **68**, 241405 (2003).
 - [10] T. Dumitrică, C. M. Landis, B. I. Yakobson, Chem. Phys. Lett. **360**, 182 (2002).
 - [11] S. V. Kalinin, V. Meunier, Phys. Rev. B **77**, 033403 (2008).
 - [12] K. S. Novoselov *et al.*, Proc. Natl. Acad. Sci. USA **102**, 10451 (2005).
 - [13] L. D. Landau, E. M. Lifshitz, *Electrodynamics of Continuous Media* (Pergamon, New York, 1993).
 - [14] R. Resta, D. Vanderbilt, Theory of polarization: A modern approach, in *Physics of ferroelectrics: a Modern perspective*, ed. by K. M. Rabe, C. H. Ahn, and J.-M. Triscone (Springer, Berlin, 2007), pp. 31-68.
 - [15] ABINIT code is a common project of the Université Catholique de Louvain, Corning Incorporated, and other contributors (URL <http://www.abinit.org>).
 - [16] S. Baroni *et al.*, <http://www.pwscf.org>.
 - [17] A.A. Mostofi *et al.* Comput. Phys. Commun. **178**, 685 (2008).
 - [18] M. Damjanović, T. Vuković, T. Milošević, B. Nikolić, Acta Cryst. **A57**, 304 (2001).
 - [19] Note that the introduced angle θ is rotated by 30° with respect to the usual chiral angle defined in the theory of carbon nanotubes, Ref. [5].
 - [20] L. D. Landau, E. M. Lifshitz, *Theory of Elasticity* (Butterworth-Heinemann, Oxford, 1995).
 - [21] Y.-H Kim, K. J. Chang, S. G. Louie, Phys. Rev. B **63**, 205408 (2001).
 - [22] D. Sánchez-Portal, E. Hernández, Phys. Rev. B **66**, 235415 (2002).
 - [23] Z. Wu, H. Krakauer, Phys. Rev. B **68**, 014112 (2003).
 - [24] S.-E. Park, T. R. Shrout, J. Appl. Phys. Cryst. **82**, 1804 (1997).
 - [25] Y. Zhang, Y.-W. Tan, H. L. Stormer, P. Kim, Nature **438**, 201 (2008).
 - [26] Z. L. Wang, J. Song, Science **312**, 242 (2006).

- [27] X. Wang, J. Song, J. Li, Z. L. Wang, Science **316**, 102 (2007).
- [28] Y. Qin, X. Wang, Z. L. Wang, Nature **451**, 809 (2008).
- [29] M. A. Schubert, S. Senz, M. Alexe, D. Hesse, U. Gösele, Appl. Phys. Lett. **316**, 122904 (2008).
- [30] M.-F. Ng, R. Q. Zhang, Phys. Rev. B **69**, 115417 (2004).
- [31] A. Y. Liu, R. Wentzcowitch, M.L. Cohen, Phys. Rev. B **39**, 1760 (1989).
- [32] K. Nakada, M. Fujita, G. Dresselhaus, M. S. Dresselhaus, Phys. Rev. B **54**, 17954 (1996).
- [33] D. Vanderbilt, R. D. King-Smith, Phys. Rev. B **48**, 4442 (1993).